Advances in Physics Theories and Applications
ISSN 2224-719X (Paper) ISSN 2225-0638 (Online)
Vol.45, 2015

Digital Image Analysis for Chemical Phase Identification and Particle Size Determination

David N Githinji
Department of Manufacturing, Industrial & Textile Engineering, Moi University,
P.O. Box 3900-30100, Eldoret, Kenya

Abstract
A methodology employing digital image analysis for chemical phase identification and particle size determination is presented. The phase of unknown iron-oxide based particulate sample was identified by analyzing its transmission electron microscope diffraction patterns and diffraction contrast images using ImageJ pattern recognition software. A standard diffraction pattern with known crystallographic spacing and a standard diffraction contrast image with known fringe spacing were used to calibrate the sample's diffraction patterns and diffraction contrast images, respectively. The phase of unknown sample was identified as iron (III) oxide with an average particle size of 8.9 nm computed from digitized binary images through thresholding process. The particles size distribution closely resembled Poisson cumulative distribution function with 61% of the particles having diameters between 1-10 nm.
Keywords: Phase identification, ImageJ, Diffraction pattern, Digital image, Particle size determination

Introduction

In recent times, it has become increasing necessary to carry out analysis on samples which are in particulate form to evaluate their morphology, chemical nature, particle size and their distribution (Mahajan, 2008). This is more important for industrial waste due to stringent disposal requirements (Woodard & Curran, 2011). The particle analysis can be carried out using transmission electron microscope (TEM) after proper sampling from the bulk (William & Douglas, 2008; Chen, et al., 2005; Akbari, et al., 2011).

In the current study, the phase and average particle size of unknown iron oxide sample was determined. The average particle size and chemical nature was determined from the analysis of TEM dark-field diffraction contrast images and diffraction patterns, respectively. The TEM micrographs were digitised and analysed using ImageJ pattern recognition software (Abramoff, et al., 2004).The digital images were stored in bitmap file-format (24-bit depth) which retains all data intact (uncompressed). The images were analysed in the JPEG file format which supports 8-bits per colour (red, green and blue) for a 24-bit total, producing relatively small files (Burger & Burge, 2009). However, image compression and repeated editing is known to degrade its quality.

The digital image allowed easy processing as they are stored as data matrix with value and location assigned to each pixel. Consequently, the data contained in the image can be displayed as histogram by plotting the pixel values (ranging from 0-255) against the number of pixels with that particular value. During image processing, the brightness is thus increased by raising the numerical value of each pixel by an equal amount while contrast is increased by maximising the difference in numerical values between highest and lowest pixels. The number of pixels used in creating the digital image determines its spatial resolution (Burger & Burge, 2009).

Methods

Iron-oxide (Fe-O) based particulate sample dispersed onto holey carbon films was observed using the Jeol 2000fx (TEM) operated at 200kV. The microscope's resolution was about 1 nm for the imaging conditions used. All the samples were observed under identical imaging and diffraction conditions with a nominal magnification of x100K. The diffraction patterns and diffraction contrast images were collected on the TEM negatives.

The negatives were obtained from reference sample (Al foil) and unknown Fe-O based particulate sample and included the dark-field images, bright-field images and diffraction patterns. The negatives were then digitised and images stored for further processing. All diffraction patterns were acquired under identical conditions of camera constant (λL) expressed as (Williams & Carter, 2009);

$$\lambda L = R_{hkl} * d_{hkl} \quad (1)$$

where; λ - wavelength of the electrons, L - camera length, R_{hkl} - diffraction pattern hkl spacing measured in real space, d_{hkl} - atomic plane spacing for a given {hkl} planes.

The reference diffraction pattern with known crystallographic spacing (d_{hkl}) was used to calibrate diffraction space. The process entailed finding the average R_{hkl} of the reference sample and multiplying it with average value of d_{hkl} to obtain camera constant. The R_{hkl} values of the unknown sample were determined from the diffraction pattern using ImageJ pattern recognition software. The camera constant was then divided by these R_{hkl} values to obtain the d_{hkl} spacings associated with the diffraction rings of the unknown Fe-O based sample.

The results were compared with the crystallographic data of known Fe-O phases and the unknown sample identified from the phase with matching d_{hkl} values. Correspondingly, its diffraction rings were indexed with Miller indices.

The dark-field contrast image of the unknown sample was calibrated using a catalase image with fringe spacing of 6.85 nm. Using ImageJ pattern recognition software, the real image scale was established. This involved dividing the length in pixels by real length in nanometre obtained by multiplying a fixed number of fringes on the catalase image with 6.85 nm.

The estimation of the average particle size was carried out on the calibrated image using ImageJ software. The image was first split into red, blue and green channels to limit the size of pixel to 255 shades of grey (8-bit depth). Correspondingly, the size of the file reduced from 17 MB to 3.5 MB. The 8-bit images were then processed through cropping and thresholding and resultant binary image analysed for particle sizes and distribution. The average diameters of the particles were determined and used in construction of histograms and cumulative frequency curves.

Results and Discussion

The diffraction pattern of the reference sample is shown in Fig. 1(a) and that of the unknown Fe-O based sample in Fig. 1(b). The diffraction patterns were obtained from the samples using Selected Area Electron Diffraction (SAED) mode of TEM. The size of the selected area determined the SAED pattern generated with spot pattern (see Fig. 1c) resulting from very small area and continuous rings patterns (see Fig. 1b) from large area. The intensities of the rings depended on the number of diffracting particles which in turn depended on the size of the selected area. For polycrystalline materials, good diffraction patterns are obtained when the selected area is as large as possible.

The diffraction contrast images of the unknown Fe-O based particulate sample under bright-field and dark-field imaging are shown in Fig. 1(d) and Fig. 1(e), respectively. The particles exhibited regular geometries. During the calibration of dark-field images a scale of 3 pixels per nm was set. Consequently, the particles with an area less than 3 pixels were considered as noise since the imaging resolution was about 1nm. The micrograph scale was found to have an error of about 10% above actual measurement. The calibration therefore improved the accuracy of the particles size measurement by similar margin.

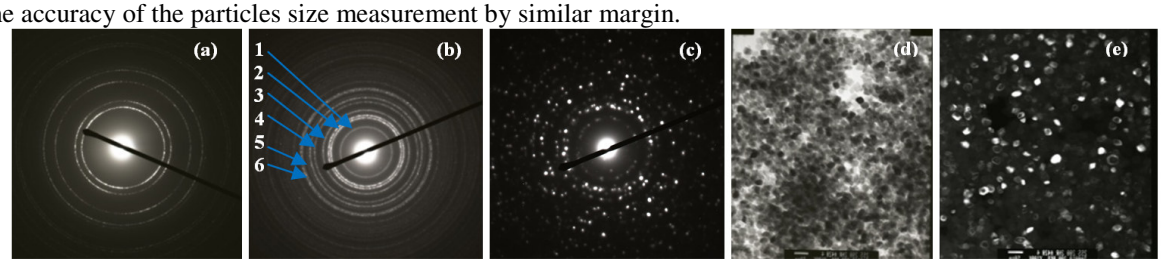

Fig. 1. TEM diffraction patterns for: (a) reference sample and (b) unknown Fe-O based sample showing TEM-SAED continuous ring pattern in (b) and spot pattern in (c). The diffraction contrast bright-field image and dark-field image for the unknown particulate sample are shown in (d) and (e), respectively.

Table 1 gives R_{hkl} and d_{hkl} values of the reference sample used in the calculation of the camera constant. Fig. 2 shows the variation of ring's intensities across the diffraction pattern of the unknown sample. The R_{hkl} values were obtained directly from the graph and this eliminated the human error associated with measuring diffraction pattern hkl spacing in real space. The sources of human error included unseen rings due to their low intensities and merged rings due to their close intensities.

Table 1: The d_{hkl}, R_{hkl} and camera constant of the reference sample (aluminium foil)

Ring	d_{hkl}	R_{hkl}	λL
1	2.3380	249.50	583.33
2	2.0248	288.00	583.14
3	1.4318	407.50	583.44
4	1.2210	478.00	583.64
5	1.1600	500.00	580.00
6	1.0124	577.00	584.15
7	0.9290	628.50	583.90

Mean	1.4453	446.93	583.09

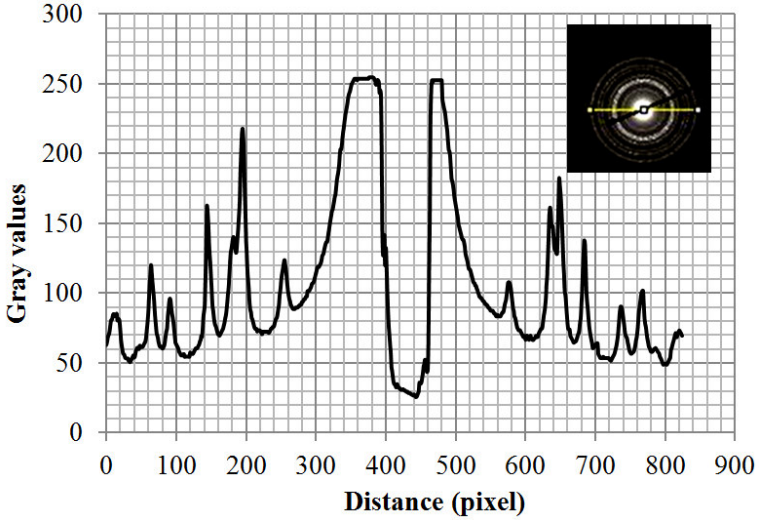

Fig. 2. The variation of diffraction rings intensities (gray values) across the diffraction pattern (insert) of the unknown sample. The low intensities rings were not detected while those with similar gray values were merged together.

Table 2 compares the measured d_{hkl} spacings of the unknown Fe-O based sample with the d_{hkl} spacings of known Fe-O phase. A close match was obtained between the two readings with minor variations which were attributed to measurement errors. Some rings were not visible due to their low intensities while other were merged together making it difficult to locate them during actual radii measurement as illustrated in Fig. 2. From the crystallographic data of known Fe-O base phases, the unknown sample was identified as iron (III) oxide (Hematite - Fe_2O_3).

Table 2: The measured and the reference d_{hkl} spacings of unknown Fe-O phase sample and the corresponding Miller indices of {hkl} planes.

Ring	Measured d-spacing	Reference d-spacing	Intensity	Hematite		
	d/Å	d/Å	I	h	k	l
1	3.6443	3.6840	30	0	1	2
2	2.6444	2.7000	100	1	0	4
3	2.4760	2.5190	70	1	1	0
4	2.1676	2.2920	3	0	0	6
5	1.8136	2.2070	20	1	1	3
6	1.6636	2.0779	3	2	0	2

Fig. 3(a) shows binary image obtained from dark-field image of unknown Fe-O based sample when the lower threshold limit gray value was set at 70. During image processing, the pixels in the 8-bit image are marked as ‘object pixels’ when their gray values is greater than some threshold value and as ‘background pixel’ when it is below. At lower threshold values, some particles agglomerate as shown by red arrows in Fig. 3 (a). This introduces error in particle size analysis as the merged particles are analysed as one big particle. However, at higher threshold values fewer particles are analysed (see Fig. 3b) and their agglomeration is reduced resulting to lower mean particle size. The accuracy of particle size analysis depends on the image thresholding and can be improved by sampling the largest area possible on the image and finding the mean particle size. Alternatively, the sample can be analysed at different threshold values and a mean particle size determined. The use of wrong scale also introduces errors in particle size analysis. During thresholding process a binary image is obtained since object pixel is given a value of ‘1’ while a background pixel is given a value of ‘0’.

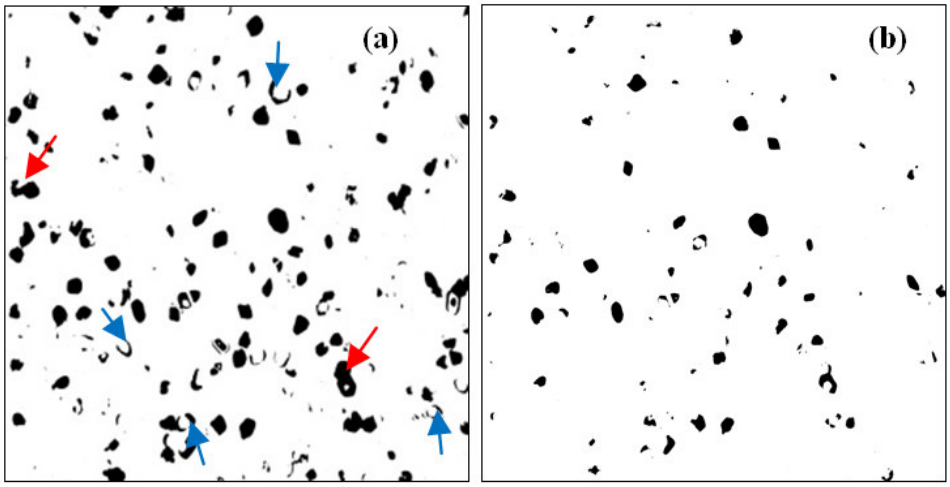

Fig. 3. The particle geometries and densities in TEM binary images obtained at (a) 70 and (b) 150 lower threshold limit gray values. The red arrows show particles that agglomerated while blue arrow shows irregularly shaped particles.

When analysing particles in the binary image using ImageJ pattern recognition software, various options are available for determining the particle sizes but only fit ellipse and centre of mass options were used. The perimeter and area options were prone to errors due to irregular shapes of some particles as shown by blue arrows in Fig. 3(a) but in general these options gave particle size distribution curves similar to that shown in Fig. 4. The errors in these options can be reduced by carrying out multiple analyses and determining the average particle sizes. The fit-ellipse option was less erroneous as it depended on the major and minor diameters of the particles. Using this option and lower threshold limit gray value of 150, the estimated average particle size was 8.9 nm. The average diameters of the largest and smallest particles were 29 nm and 1 nm, respectively. Fig. 4 shows the particles size distribution curve which closely resembles the Poisson cumulative distribution function as it depended on the probability that the particle sizes were greater than a lower threshold limit and less than an upper threshold limit. It can be noted that 61% of the particles had diameters between 1- 10 nm and only 4.5% had diameters above 20 nm.

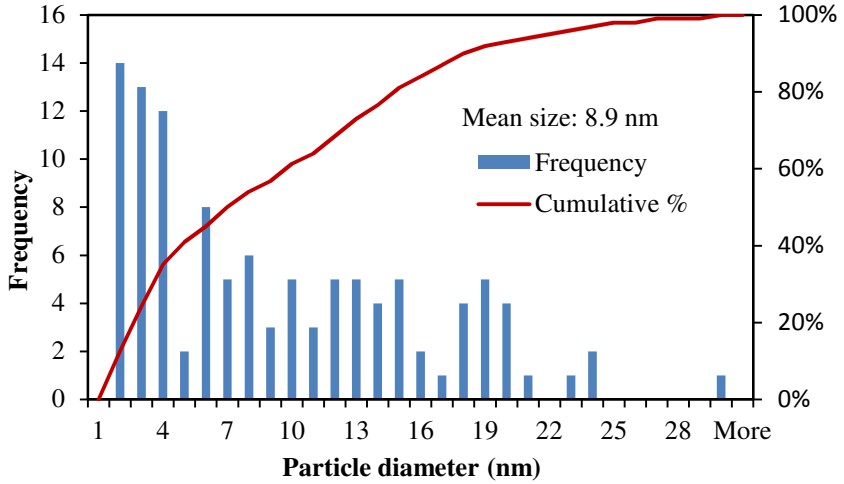

Fig. 4. The histogram and cumulative frequency curve of particle size distribution when analyzed using fit-ellipse option. Similar curves were obtained when analysis was done based on the area, perimeter and centre of mass options.

Conclusions

The digital analysis of the diffraction patterns and diffraction contrast images using ImageJ pattern recognition software enabled determination of the unknown sample chemical phase as the iron (III) oxide and the average particle size as 8.9 nm. It was found that the particles size distribution closely resembled Poisson distribution function with 61% of the particles having diameters between 1-10 nm. The use was made of standard diffraction patterns with known crystallographic spacing and standard diffraction contrast image with known fringe spacing for calibration of the sample's diffraction patterns and diffraction images.

References

Abramoff, M., J, M. P. & J, R. S., 2004. Image processing with ImageJ. *Biophotonics international,* 11(7), pp. 36-42.

Akbari, B., Tavandashti, M. P. & Zandrahimi, M., 2011. Particle size characterization of nanoparticles - A practical approach. *Iranian Journal of Materials Science & Engineering,* 8(2), pp. 48-56.

Burger, W. & Burge, M. J., 2009. *Digital Image Processing: An Algorithmic Introduction Using Java.* s.l.:Springer Science & Business Media.

Chen, Y., Shah, N., Huggins, F. & Huffman, G., 2005. Transmission electron microscopy investigation of ultrafine coal fly ash particles. *Environmental Science and Technology,* 39(4), pp. 1144-1151.

Mahajan, S., 2008. *Pollution Control In Process Industries.* New Delhi: Tata McGraw-Hill.

William, D. & Douglas, B. J., 2008. Particle Size Determination Using TEM: A Discussion of Image Acquisition and Analysis for the Novice Microscopist. *Langmuir,* 24(20), p. 11350–11360.

Williams, D. B. & Carter, C. B., 2009. *Transmission Electron Microscopy: A Textbook for Materials Science, Volume 3.* s.l.:Springer Science & Business Media.

Woodard & Curran, I., 2011. *Industrial Waste Treatment Handbook.* s.l.:Butterworth-Heinemann.

The IISTE is a pioneer in the Open-Access hosting service and academic event management. The aim of the firm is Accelerating Global Knowledge Sharing.

More information about the firm can be found on the homepage:
http://www.iiste.org

CALL FOR JOURNAL PAPERS

There are more than 30 peer-reviewed academic journals hosted under the hosting platform.

Prospective authors of journals can find the submission instruction on the following page: http://www.iiste.org/journals/ All the journals articles are available online to the readers all over the world without financial, legal, or technical barriers other than those inseparable from gaining access to the internet itself. Paper version of the journals is also available upon request of readers and authors.

MORE RESOURCES

Book publication information: http://www.iiste.org/book/

Academic conference: http://www.iiste.org/conference/upcoming-conferences-call-for-paper/

IISTE Knowledge Sharing Partners

EBSCO, Index Copernicus, Ulrich's Periodicals Directory, JournalTOCS, PKP Open Archives Harvester, Bielefeld Academic Search Engine, Elektronische Zeitschriftenbibliothek EZB, Open J-Gate, OCLC WorldCat, Universe Digtial Library , NewJour, Google Scholar